Scaling of flat band potential and dielectric constant as a function of Ta concentration in Ta-TiO_2 epitaxial films

Y. L. Zhao,[1,2] A. Roy Barman,[1,2] S. Dhar,[1,3] A. Annadi,[1,2] M. Motapothula,[1,2] Jinghao Wang,[4] Haibin Su,[4] M. Breese,[1,2] T. Venkatesan,[1,2,3,a] and Q. Wang[1,5,b]

[1]*NUSNNI-NanoCore, National University of Singapore, 117411, Singapore*
[2]*Department of Physics, National University of Singapore, 117542, Singapore*
[3]*Department of Electrical and Computer Engineering, National University of Singapore, 117576, Singapore*
[4]*Division of Materials Science, Nanyang Technological University, 639798, Singapore*
[5]*Department of Materials Science and Engineering, National University of Singapore, 117576, Singapore*

(Received 21 February 2011; accepted 7 June 2011; published online 29 June 2011)

Electrochemical impedance spectroscopy measurements of pulsed laser deposited single crystal anatase TiO_2 thin films with various concentrations of Ta substituting for Ti were carried out. The qualities of the films were characterized by X-ray diffraction and Rutherford back scattering-channeling measurements. UV-visible measurements show a systematic increase of the bandgap with Ta incorporation. Corresponding Mott-Schottky plot was applied to obtain a continuous shift of the flat band potential with increasing free charge carrier (provided by Ta) concentration. This was verified theoretically by *ab initio* calculation which shows that extra Ta *d*-electrons occupy Ti t_{2g} orbital with increasing Ta concentration, thereby pushing up the Fermi level. The Mott-Schottky results were consistent when compared with Hall effect and temperature dependent resistivity measurements. From the measured deviation of carrier densities from Hall and Mott-Schottky measurements we have estimated the static dielectric constant of the TiO_2 as a function of Ta incorporation, not possible from capacitive measurements. [doi:10.1063/1.3609927]

I. INTRODUCTION

TiO_2, as a wide band gap *n*-type semiconducting transition metal oxide, has attracted a lot of attention for various optoelectronic applications such as transparent conducting oxide (TCO),[1] photoelectrode for solar cells,[2] photocatalyst for water treatment,[3] etc., because of its superior optical and electrical properties. Among these applications, TiO_2 has been extensively studied as the photoanode of dye-sensitized solar cells (DSCs). Recently metal-doped TiO_2 has been found to present improved performance in DSCs as compared to pure TiO_2 films.[4–6] For instance, higher power conversion efficiency of DSCs was observed with Nb-doped TiO_2 mesoscopic film as a result of improved open circuit photovoltage and short circuit photocurrent.[4] In addition, improved charge transfer and collection characteristics were demonstrated when Nb-doped TiO_2 was employed as hole blocking layer underneath the mesoscopic film.[5] Besides their application as photoelectrode, Ta and Nb-doped TiO_2 films deposited on non-alkali glass by Pulsed laser deposition (PLD) were reported to give slightly lower room temperature resistivity ($\rho_{RT} \sim 1.5\times10^{-3}\ \Omega\cdot$cm) and comparable transparency (60-80% in the visible region) to the commercial TCOs, such as tin doped indium oxide (ITO) and fluorine-doped tin dioxide (FTO),[6] making these doped TiO_2 promising materials for transparent

[a]Electronic mail: venky@nus.edu.sg.k
[b]Electronic mail: qing.wang@nus.edu.sg

conducting oxides. Since most of these applications are related to the electrical and optical properties of TiO_2 films and hence closely related to the band structure of the material, knowledge of band gap and band edges of the doped TiO_2 films would be very useful for making efficient and low-cost devices. Recently, Lu *et al.* reported a positive shift of the flat band potential of nanocrystalline Nb-doped TiO_2 film.[4] However, the presence of a large density of surface states at the grain boundaries may deplete and kill the space charge region throughout the film, hence reducing the effectiveness of the electrode. Further in this regime the application of Mott-Schottky equation might not be valid any more.[7] To address this issue, it was proposed that epitaxial film rather than polycrystalline porous film should be used.[8] In the present work, we have used the model system of pulsed laser deposited Ta incorporated anatase TiO_2 epitaxial thin films to examine the shift of band positions as a function of Ta concentration.

UV-vis measurements show a systematic increase of the bandgap with Ta incorporation. Corresponding Mott-Schottky plot was applied to obtain a continuous shift of the flat band potential with increasing free charge carrier (Ta) concentration.[9,10] This was verified theoretically by *ab initio* calculation which show that extra Ta *d*-electrons occupy Ti t_{2g} orbital with increasing Ta concentration, thereby pushing up the Fermi level. The Mott-Schottky results were consistent when compared with Hall effect and temperature dependent resistivity measurements. From the measured deviation of carrier densities from Hall and Mott-Schottky measurements, the static dielectric constant of the TiO_2 as a function of Ta incorporation was estimated.

II. EXPERIMENTAL SECTION

Single crystal $Ti_{1-x}Ta_xO_2$ (x = 0.0, 0.015, 0.035, 0.064 and 0.089) films were deposited by pulsed laser deposition (PLD) technique on single crystal (001) $LaAlO_3$ substrates (LAO). The PLD targets were prepared by solid-state reaction of 99.999% pure TiO_2 and 99.995% pure Ta_2O_5 powders (bought from Sigma Aldrich Co.). A Lambda Physik pulsed excimer laser (λ = 248 nm) with energy density of 1.8 J/cm^2 with a frequency of 5 Hz was used for the target ablation. Target to substrate distance was about 7 cm inside the vacuum chamber. The oxygen partial pressure during deposition was maintained at 1×10^{-5} Torr with chamber base pressure below 1×10^{-6} Torr and the deposition temperature was maintained at 700 ^{o}C. The deposition lasted one hour with 5 Hz laser frequency giving around 200 nm thick films. After the deposition, all the samples were annealed in atmosphere at 500 ^{o}C for 1 hour to minimize the effect of oxygen vacancy.

Crystal structures of all the films were examined by XRD technique using Bruker D8 Discover ($Cu_{K\alpha}$ = 1.54060 Å) system. The quality of single crystal films and its thickness, Ta concentrations, Ta substitution inside the Ta incorporated TiO_2 films were determined by RBS-Channeling technique. The light absorbance and transmittance of the films were studied in the UV–vis regime using a Shimadzu Solidspec-3700 spectrophotometer. Hall effect and temperature dependence of resistivity (R-T) were measure using a physical property measurement system (Quantum Design). The experimental results are shown in Fig. 1.

The electrochemical impedance measurements (EIS) were carried out using these well-characterized Ta incorporated TiO_2 single crystal films on the LAO substrate. As shown in Fig. 2(a), the top of film was covered by a 100 nm thick Al layer deposited by thermal evaporation leaving the central part uncovered. A Cu wire was connected to the Al contact pad by silver paint. Then the pads were covered by EPOXY for an electric isolation.

For the EIS measurement, three electrode configurations was used: the working electrode was the TiO_2 sample (Fig. 2(a)); the counter electrode was a Pt wire and the reference electrode was made of 0.01 M $AgNO_3$/Ag, 0.1 M Tetrabutylammonium perchlorate (TBAP) dissolved in anhydrous acetronitrile (99.9% pure). The potential of the reference electrode was calibrated relative to Ferrocene using cyclic voltammetry (CV) measurement. The obtained $E_{1/2}$ of Ferrocene is around 0.08 V with respect to Ag/$AgNO_3$ reference electrode and was stable during the experiment. The electrolyte used in the present experiment was 0.1 M TBAP in anhydrous acetronitrile (99.9% pure). The impedance measurements were carried out with a Potentiostat equipped with a frequency

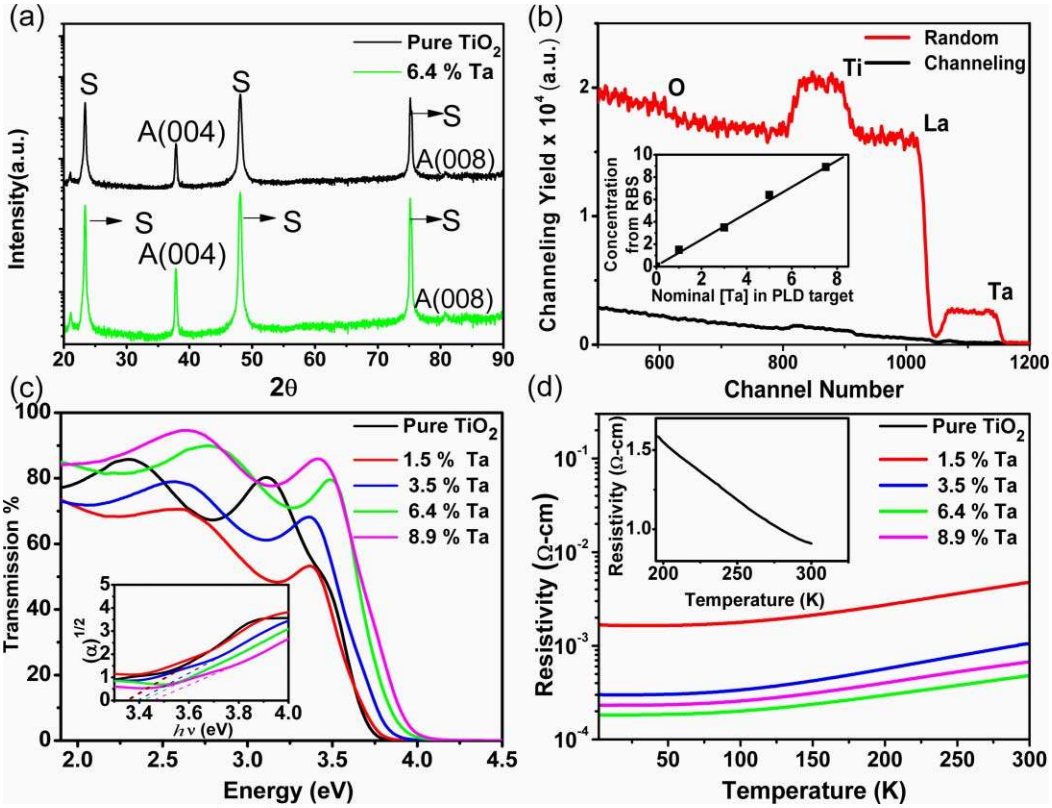

FIG. 1. (a) Typical XRD spectra of pure anatase and 6.4% Ta incorporated TiO_2 thin films deposited by pulsed laser deposition, where label A indicates anatase phase, S indicates substrate. (b) Random and channeling spectra of 6.4% Ta-TiO_2 film showing excellent channeling yield. Ta concentration measured by RBS versus nominal Ta concentration in the PLD target is shown in the inset. (c) UV-vis transmission spectra of pure and Ta-TiO_2 samples. The inset shows the Blue shift with Ta incorporation. (d) Resistivity vs. temperature of Ta-TiO_2 films as a function of Ta concentration.

response analyzer (AUTOLAB PGSTAT302N) in the frequency range from 0.1 Hz (0.01 Hz for the pure TiO_2 sample) to 10^5 Hz.

III. RESULTS AND DISCUSSIONS

Fig. 1(a) shows the typical X-ray diffraction (XRD) patterns of pure and 6.4% Ta incorporated TiO_2 films confirming the formation of an anatase phase. Besides the signals come from the substrate, only Anatase (004) and Anatase (008) can be seen in the spectrum. The TiO_2 films for all Ta concentration showed pure anatase phase and after annealing in atmosphere good stability over a period of six months. In fact, the Ta incorporated TiO_2 was found to be an alloy with a different band structure compared to their parent materials.[11] In the Rutherford backscattering (RBS) spectrum (Fig. 1(b)), the Ta peak is separated from La and Al (from substrate), Ti (from film) and oxygen edges due to their atomic mass differences, from which, Ta concentration can be simulated accurately. RBS-Channeling spectra of these samples, as depicted in Fig. 1(b), clearly shows a low channeling minimum yield for Ti and La (∼2%) which implies that the Ti is epitaxially aligned with the substrate. Almost all Ta ions were uniformly substituted (channeling minimum yield 2.5%) in the Ti lattice. The typical thickness of the films was found to be about 200 nm. The amount of Ta concentration in the films was determined and plotted in the inset of Fig. 1(b) as a function of nominal Ta concentration in the PLD target. The measured RBS film concentration of Ta deviated systematically within 10-20% of the nominal target concentration but in our subsequent data we used only the Ta concentration measured by RBS.

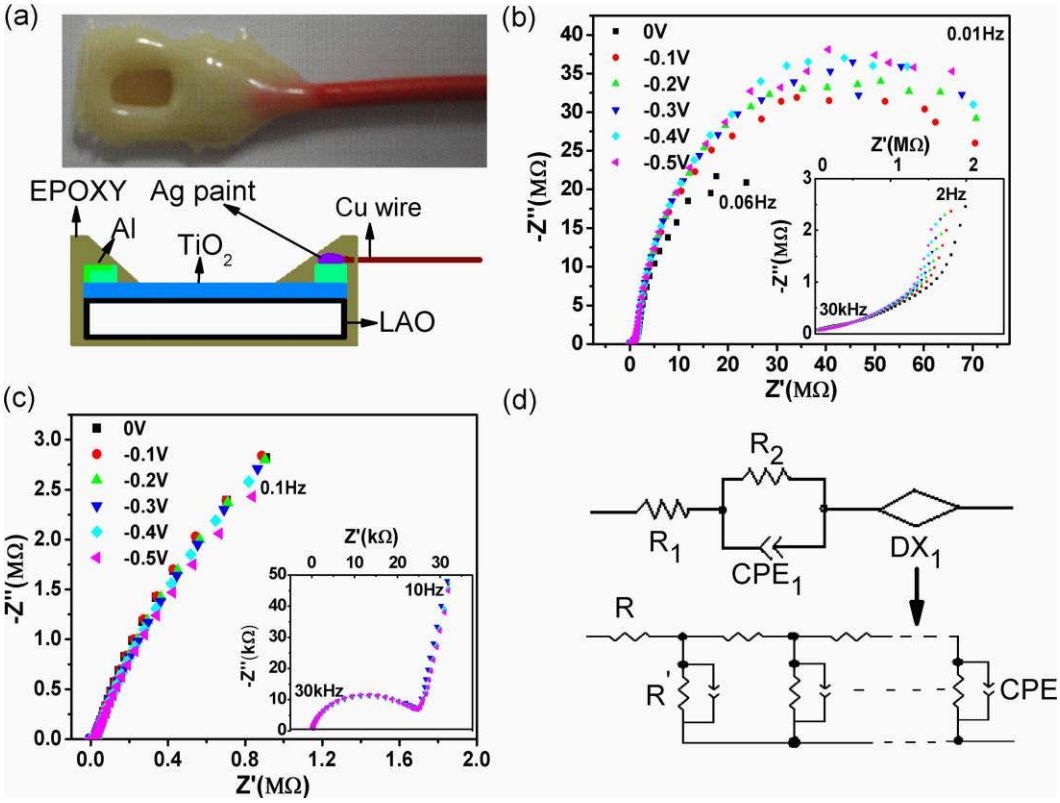

FIG. 2. (a) Schematic graph of the TiO_2 samples used in the impedance measurement and a photo of actual device. (b) Nyquist plots of pure TiO_2 with Al contact layer. The frequency range here is from 0.01 Hz to 30 kHz. The inset graph is in the expanded scale of the high frequency data. (c) Nyquist plots of 1.5% Ta incorporated TiO_2 without Al buffer contact layer. The frequency range shown here is from 0.01 Hz to 30 kHz. The inset graph is the expanded scale of the high frequency data. (d) Equivalent circuit of the samples and DX_1.

The transmission spectra of the prepared samples (normalized for the LAO substrate) measured by UV-vis spectroscopy are shown in Fig. 1(c). The spectra were fitted using the equation $\alpha \propto (h\nu - E_g)^2$ for an indirect band gap for finding the optical band gap energy (E_g) of the samples,[12] where α is the inverse absorption length. The band gap energy for pure anatase TiO_2 is determined to be 3.35 eV. In comparison, with increasing Ta concentration the optical band gap was blue shifted, obeying Vegard's Law.[13,14]

Fig. 1(d) shows the temperature dependence of the resistivity of various Ta incorporated TiO_2 films. It is clear that the resistivity of pure anatase TiO_2 film decreases with temperature (inset of Fig. 1(d)) indicating semiconducting behavior. In contrast, all the Ta incorporated TiO_2 samples are metallic with resistivity increasing with temperature. The room temperature minimum resistivity was 4.7×10^{-3} $\Omega\cdot$cm, which was obtained with 6.4% Ta-TiO_2 film.

Fig. 2(a) shows a photograph and the schematic diagram of the working electrode made of these TiO_2 films. The electrochemical impedance spectra of a pure anatase TiO_2 thin film measured at different potentials are shown in Fig. 2(b), where a big semicircle is seen in the low frequency range. However, with the magnified spectra (shown in the inset), a much more complex impedance response is seen to develop in the high frequency region. A similar situation was observed with Ta incorporated TiO_2 when a thin Al layer was deposited to make electrical contact. However, when the Al contact was removed and replaced with Ag paint, only a simple semicircle was seen in the high frequency region. Fig. 2(c) shows the impedance spectra obtained with 1.5% Ta-TiO_2 without the Al contact layer. As shown in the inset, besides a big semicircle seen in the low frequency region, a much smaller semicircle with almost constant diameter was observed at higher frequency.

These data can be fitted using an equivalent circuit shown in Fig. 2(d). Here, R_1 represents the series resistance of the circuit. R_2 and the constant phase element, (CPE_1) arise from the contact of Al or Ag paint with TiO_2 film. The DX_1 is a transmission line circuit element (Fig. 2(d)) comprising of three parts: Sheet resistance R of the TiO_2 film, the space charge layer capacitance, CPE and resistance R′ arising from the leakage of current. For pure TiO_2 films, the Warburg impedance is unambiguously seen in the intermediate frequency range, indicating a distinguishable electron transport process through the thin films (R). A transmission line model was employed to fit the spectra.[15,16] Evidently the sheet resistance R decreases gradually with the applied forward bias, which can be rationalized based upon the evolution of depletion layer with bias. With increasing forward bias, the height and width of depletion layer shrink. As a result, charge transport through the film is facilitated. In contrast, as R is much smaller than R_2 and R′ in Ta-TiO_2 films, the straight line of Warburg impedance is not distinguishable in the spectra. However, since the space charge layer capacitance was obtained from the low frequency part, the fitting will not be compromised by the different electron transport kinetics in the intermediate frequency range. So the data can be fitted with the simple parallel R′-CPE model. To obtain the true space charge layer capacitance value, the obtained CPE capacitance value was then corrected by the following equation:[17]

$$C = T\left(\omega''_{\max}\right)^{P-1} \tag{1}$$

where C is the corrected capacitance, $\omega''_{\max}$ represents the frequency of maximum $-Z''$ value on the Nyquist plot, T and P come from the definition of the impedance of CPE, i.e., $Z_{CPE} = T^{-1}/(\omega i)^P$. Equation (1) is derived from the correction of parallel connection of a CPE and resistor, and used here because the semicircle in the lower frequencies can be simplified as a parallel circuit of a resistor and a CPE. In addition, the two semicircles are separated clearly from each other, as shown in Fig. 2(c), which make the fitting more reliable.

In order to determine the flat band potentials of the samples relative to $Ag/AgNO_3$ reference electrode, Mott-Schottky equation (depending on the free charge carrier density) was derived from the Poisson's equation for Schottky barriers at semiconductor/metal and semiconductor/electrolyte heterojunctions with the assumptions of perfect blocking properties of the barrier, absence of surface states, dominant space charge layer capacitance rather than Helmholtz layer capacitance, perfect planar interface, zero resistance of the metal and electrolyte.[7] For pure anatase TiO_2 (the free charge carrier density is smaller than 10^{19} cm^{-3}), the ideal Mott-Schottky equation obtained by applying Boltzmann statistics is written as:[9,10]

$$\frac{1}{C^2} = \frac{2}{e\varepsilon_0\varepsilon_r N_{sc} A^2}\left(V - V_{fb} - \frac{k_B T}{e}\right) \tag{2}$$

where C is the space charge layer capacitance, ε_0 is the vacuum permittivity, $\varepsilon_r = 31$ is the static dielectric constant of anatase TiO_2,[18,19] N_{sc} is the charge density in the space charge region, A is the exposed area of the sample to the electrolyte, V is the applied potential with respect to reference electrode, V_{fb} is the flat band potential, k_B is the Boltzmann constant, T is the absolute room temperature, and e is the elementary charge of electron.

For the Ta-TiO_2 samples, as the free charge carrier density is larger than 10^{19} cm^{-3}, one cannot apply Boltzmann statistics due to metal-like conducting property with significant carrier degeneracy. Instead, a modified Mott-Schottky equation was derived by applying a more general Fermi-Dirac statistics and is given below:[20]

$$\frac{1}{C^2} = \frac{2}{e\varepsilon_0\varepsilon_r N_{sc} A^2}\left(V - V_{fb} - \frac{2}{5}\frac{E_F}{e}\right) \tag{3}$$

where $E_F = \frac{\hbar^2(3\pi^2 N)^{2/3}}{2m^*}$ is the Fermi level energy, m^* is the effective electron mass. It should be noted that the difference in the flat band potential using the above two equations is negligible when free charge carrier density is smaller than 5×10^{20} cm^{-3}.[20]

With the corrected CPE at different potentials, Mott-Schottky relations for the pure and Ta incorporated TiO_2 electrodes were plotted in Fig. 3, where it is assumed that the space charge layer capacitance is much smaller than Helmholtz layer capacitance and is dominant at low bias voltage.[21] By applying Mott-Schottky equations, the flat band potentials were estimated and are shown in the

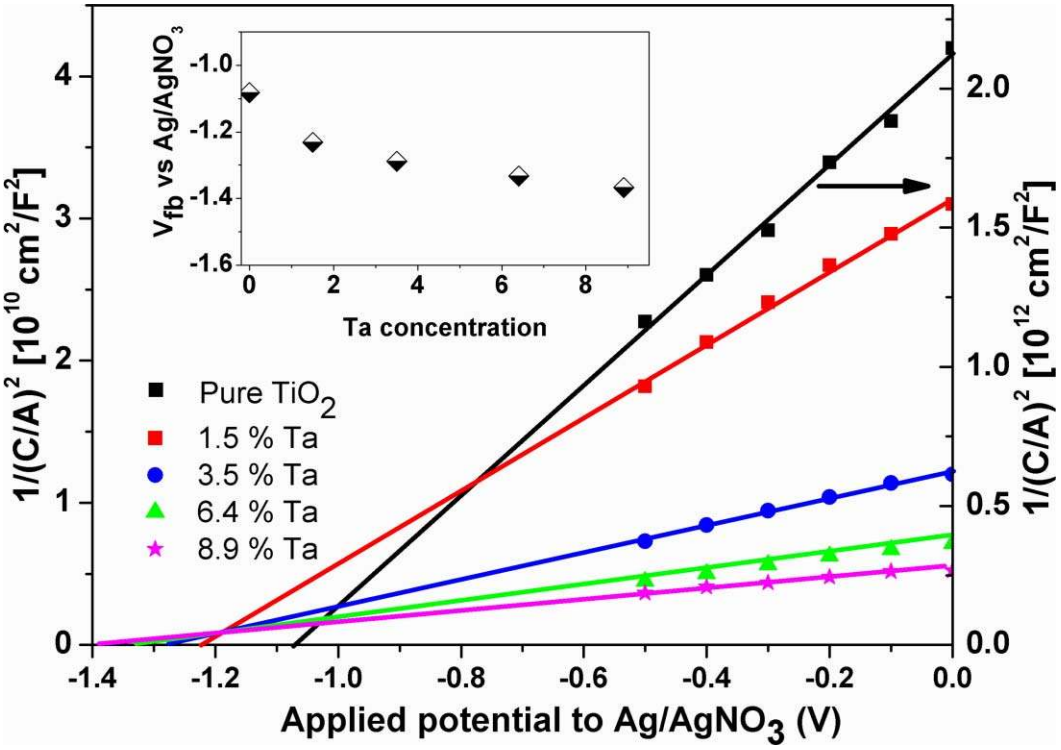

FIG. 3. Mott-Schottky plot of the samples. Right y-axis is for pure TiO_2, left y-axis is for Ta-TiO_2 samples. X-axis is the applied potential to the samples relative to the reference electrode. The straight lines were drawn by eyes. The inset graph is the flat band potential of the samples obtained from the Mott-Schottky equations by considering the applied potential plot.

inset of Fig. 3. It is clear that the pure anatase TiO_2 possesses the least negative flat band potential of $\sim$ -1.08 V (vs. $Ag/AgNO_3$). As the Ta concentration increases, the flat band potential of the sample becomes more negative.

The free charge carrier concentration was determined from the slope of the Mott-Schottky plots in Fig. 3. With increasing Ta concentration in TiO_2, free charge carrier density increases, and as a result the sheet resistance of the Ta incorporated thin films drops gradually. These data are plotted in Fig. 4(a) along with those obtained from the Hall effect and direct resistivity measurements. From both the impedance and Hall effect measurements, the free charge carrier density was found to increase with Ta concentration. However, the free charge carrier density determined by Hall effect measurement becomes larger than that obtained from impedance measurement at higher Ta concentration. The discrepancy between these two measurements is most likely from the change of the static dielectric constant when pure anatase TiO_2 films are incorporated with Ta. Since the impedance measurement assumed ε_r of 31 for all the films by reconciling the two carrier density data we may be able to estimate the ε_r as a function of Ta concentration.

As the free charge carrier density can be independently obtained from Hall effect measurement, by substituting it into Mott-Schottky equation the static dielectric constant can be calculated from the equation:

$$\varepsilon_r = \frac{2}{e\varepsilon_0 d_{M-S} N_{SC}^{Hall} A^2} \tag{4}$$

where $d_{M\text{-}S}$ is the slope of the linear part of Mott-Schottky plot, N_{SC}^{Hall} is the free charge carrier density determined by Hall effect measurement.

As revealed in Fig. 4(b), the dielectric constants of the pure and Ta incorporated samples were calculated with equation (4). The static dielectric constant of the pure anatase TiO_2 was calculated to be $\sim$32, very close to the reported value of 31,[18,19] which validates the above approach. As Ta

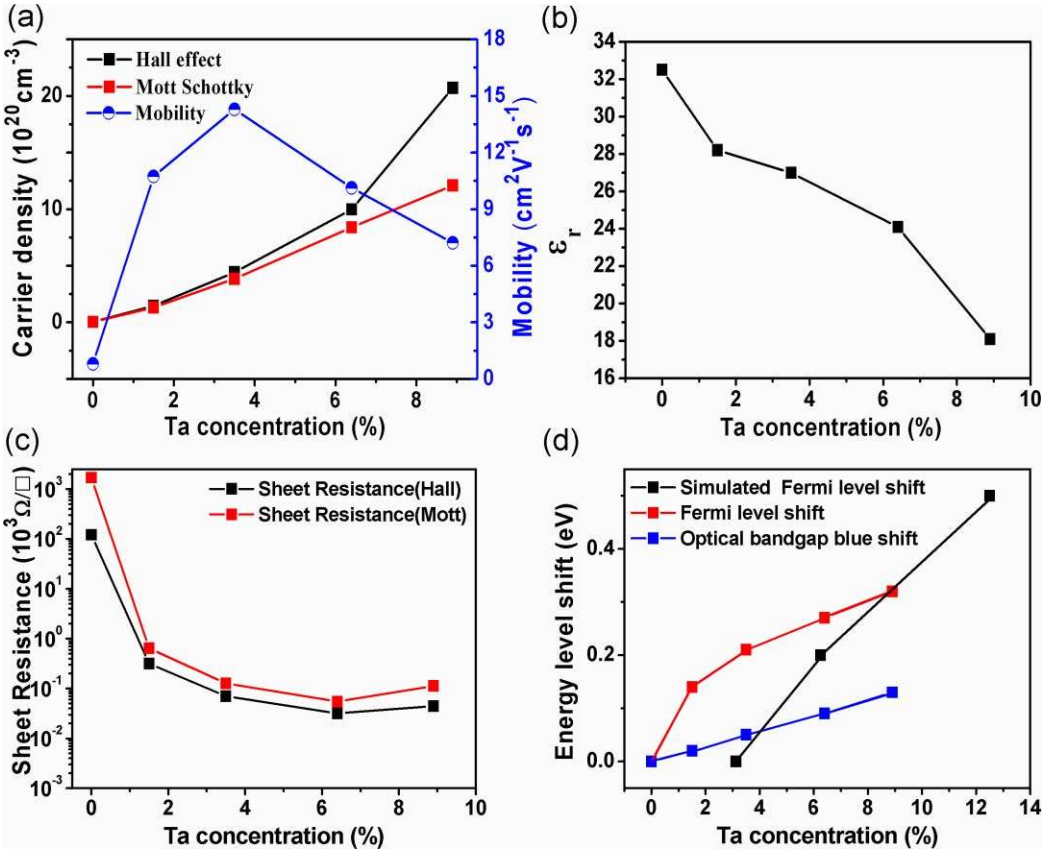

FIG. 4. (a) Hall effect measurement of the carrier density (black) and mobility (blue) and carrier density estimated from Mott-Schottky plot (red). (b) Dielectric constant as function of measured Ta concentration calculated by reconciling Hall effect and Mott-Schottky measurements of carrier densities. (c) Comparison of Sheet resistance of the films as function of measured Ta concentration from direct resistivity versus from Mott-Schottky plot. (d) Experimentally obtained Fermi level (red) and optical band gap blue shift of the Ta incorporated TiO_2 samples where pure TiO_2 was selected as the reference point (blue), and simulated Fermi level shift with measured Ta doping concentration (black), the first point (3.125%) is set as zero for easy comparison.

atoms were incorporated into the film, the dielectric constant of the sample decreased gradually. In the present experiment, as the space charge layer capacitance was obtained from the low frequency region of impedance spectra, we assume the derived dielectric constant to be approximately the static dielectric constant. In general, the static dielectric constant of insulating material is determined by measuring the capacitance of the insulating materials sandwiched between two metal plates. However, when the material becomes relatively conducting, it becomes difficult to get reliable measurement using low frequency alternating current. Hence the above method of combining Hall effect and Mott-Schottky measurements provides a feasible way of determining the static dielectric constant of metallic material.

As shown in Fig. 4(a), the Hall mobility of the samples initially increases with Ta concentration and then drops after it gets to a maximum at about 4-5%. Fig. 4(c) shows the sheet resistance obtained from Hall effect measurement showing good consistence with impedance measurement. At room temperature it decreases with increasing Ta concentration and saturates at high Ta concentration. The energy difference between the conduction band edge and the Fermi level of pure anatase can be approximated by the following equation:

$$\Delta E = k_B T \ln\left(\frac{N_{sc}}{N_c}\right) \tag{5}$$

where $N_c = 2(\frac{m_c{}^* k_B T}{2\pi\hbar^2})^{2/3}$ is the effective density of states for the conduction band. Assuming the effective electron mass $m_c{}^*$ in anatase TiO_2 is 1 m_0 (m_0 is free electron mass);[22] the Fermi level at room temperature was estimated to be about 62 meV below the conduction band edge. To address the movement of the Fermi level and the changes of the rigid band gap due to Ta incorporation in TiO_2 films, the shift of the flat band potential and optical band gap need to be considered concurrently. If we assume that the valence band edge is not moving with Ta incorporation and that only Fermi level and conduction band edge are shifting, the observed results become difficult to explain. As can be seen in Fig. 4(d), at 1.5% Ta level, the optical band gap only blue shifts ~20 meV. However, the Fermi level has shifted ~140 meV. At this level, the sample is already degenerate, which means the excited electron by photons can no longer occupy the lowest state of the conduction band. Hence the optical band gap blue shift value should be much larger than 20 meV, which disagrees with the experimental result. So the valence band must shift to higher energies to reconcile the difference between the measured movement of the Fermi level and the observed blue shift of the optical band gap. Based on this assumption, the Ta incorporated TiO_2 reaches degeneracy at about 0.8% Ta substitution (at the degeneracy point, the Fermi level and conduction band edge just overlap).

In order to verify our experimental findings, we performed plane-wave pseudopotential Density Function theory (DFT) calculations for Ta incorporated anatase TiO_2. The calculation with the Vienna *ab initio* Simulation Package (VASP) code[23,24] used generalized gradient approximation with Perdew-Burke-Ernzerhof exchange-correlation functional.[25] The oxygen $2s^2 2p^4$, titanium $3d^2 4s^2$ and tatanlum $5d^3 6s^2$ are treated as valence electrons. We used the projector augmented-wave (PAW) potential,[26] which is generally more accurate than the ultrasoft pseudopotential, and the plane-wave cut-off is set as 500 eV based on convergence test. The Ta concentration is simulated from 3.125% to 12.5% by using TiO_2 supercell from $2\times1\times1$ to $2\times2\times2$. All the atom positions are allowed to relax until the force acting on each is less than 0.02 eV/Å. Our simulated crystal structure of anatase TiO_2 (a = 3.80 Å, c = 9.72 Å) matched well with experimental data (a = 3.80 Å, c = 9.61 Å),[27] which also proved the credibility of our simulation. From Fig. 4(d) we can see that the trend for simulated Fermi level shift agrees well with observed experimental data: Fermi level moves up with increasing Ta concentration. Further partial density of state analysis showed that the *d*-orbital energy of Ta is nearly the same as that of Ti. Substituting Ti with Ta will transfer their excess *d*-electron into the conduction band minimum (CBM) instead of introducing intermediate states in the band-gap. When the Ta concentration is increased, the Fermi level is pushed further up from the CBM by the excess Ta-*d* electrons. We noticed the slope difference of Fermi level shift between simulated and experimental data. It origins from discrepancy between simulation premises based on perfect infinite three-dimensional bulk supercell and actual experiment condition limitation, but it doesn't influence the derived conclusion here. Further work is to be done in order to get better quantitative match with experimental data and theory.

In summary, for studying the flat band potential, thin epitaxial $Ti_{1-x}Ta_xO_2$ (where x = 0.0, 0.015, 0.035, 0.064 and 0.089) films were deposited on (001) $LaAlO_3$ substrate at 700 °C in oxygen partial pressure of 1×10^{-5} Torr by pulsed laser deposition technique. Almost all the Ta was found to be substituted in the Ti sites by ion channeling measurements. Continuous shift of the flat band potential of Ta incorporated anatase TiO_2 with increasing Ta concentration was observed from the Mott-Schottky plots. The DFT calculation confirmed the continuous shift of the Fermi level. The obtained free charge carrier density and room-temperature sheet resistance are consistent with those obtained from the Hall effect and direct resistivity measurements. The free charge carrier density increased with increasing Ta concentration and the sheet resistance decrease with Ta saturating at higher concentration. By reconciling the carrier density measurements from Hall and Mott-Schottky plot we were able to estimate the static dielectric constant of metallic Ta incorporated TiO_2, a measurement which is difficult to accomplish via capacitive measurements. By considering the blue shift of the optical band gap together with the movement of the Fermi level, significant movement of the valence band was recognized and the formation of the degenerate states was estimated at the Ta concentration of 0.8%.

ACKNOWLEDGMENTS

We very much appreciate all the help provided during the Al contact deposition by Dr. Ouyang's group at NUS. We are also very thankful to Dr. James R. Jennings for helping in the EIS measurements. This work is supported by NUSNNI-Nanocore start-up fund and NRF-CRP grants "Tailoring Oxide Electronics by Atomic Control" (NRF2008NRF-CRP002-024). The theoretical work performed at NTU is supported in part by a MOE AcRf-Tier-1 grant (no. M52070060) and A*STAR SERC grant (no. M47070020)

[1] C. Euvananont, C. Junin, K. Inpor, P. Limthongkul, C. Thanachayanont, Cermics Int. **34**, 1067 (2008).
[2] B. O'Regan, M. Gratzel, Nature **353**, 737 (1991).
[3] A. Fujishima, K. Honda, Nature **283**, 37 (1972).
[4] X. J. Lu, X. L. Mou, J. J. Wu, D. W. Zhang, L. L. Zhang, F. Q. Huang, F. F. Xu, and S. M. Huang, Adv. Func. Mater. **20**, 509 (2010).
[5] S. Lee, J. H. Noh, H. S. Han, D. K. Yim, D. H. Kim, J. K. Lee, J. Y. Kim, H. S. Jung and K. S. Hong, J. Phys. Chem. C **113**, 6878 (2009).
[6] T. Hitosugi, A. Ueda, Y. Furubayashi, Y. Hirose, S. Konuma, T. Shimada, and T. Hasegawa, Jap. J. Appl. Phys. **46**, L86 (2007).
[7] F Cardon, WP Gomest, J. Phys. D: Appl. Phys. **11**, L67 (1978).
[8] F. Fabregat-Santiago, G. Garcia-Belmonte, J. Bisquert, P. Bogdanoff, and A. Zaban, J. Electrochem. Soc. **150**, E293 (2003).
[9] W. Schottky, Z. Phys. **113**, 367 (1939); **118**, 539 (1942).
[10] N. F. Mott, Proc. R. Soc. A **171**, 27 (1939).
[11] A. Roy Barman, M. Motapothula, A. Annadi, K. Gopinadhan, Y. L. Zhao, Z. Yong, I. Santoso, Ariando, M. Breese, A. Rusydi, S. Dhar and T. Venkatesan. Appl. Phys. Lett. **98**, 072111 (2011)
[12] J. R. Simpson and H. D. Drew, Phys. Rev. B **69**, 193205 (2004).
[13] A. R. Denton and N. W. Ashcroft, Phys. Rev. A **43**, 3161 (1991).
[14] J. W. Strane, H. J. Stein, S. R. Lee, B. L. Doyle, S. T. Picraux, and J. W. Mayer, Appl. Phys. Lett. **63**, 2786 (1993).
[15] J. Bisquert, G. Garcia-Belmonte, F. Fabregat-Santiago, A. Compte, Electrochem. Commun. **1**, 429 (1999).
[16] J. Bisquert, Phys. Chem. Chem. Phys. **2**, 4185 (2000).
[17] C. H. Hsu, F. Mansfeld, Corrosion **57**, 747 (2001).
[18] A. Euken and U. A. Büchner, Z. Phys. Chem. B **27**, 321 (1934).
[19] S. Roberts, Phy. Rev. **76**, 1215 (1949).
[20] A. M. Sukhotin, M. S. Grilikhes, E. V. Lisovaya, Electrochim. Acta **34**, 109 (1989).
[21] A. Hassanzadeh, M. H. Habibi, A. Zeini-Isfahani, Acta Chim.Slov. **51**, 507 (2004).
[22] D. Kurita, S. Ohta, K. Sugiura, H. Ohta, and K. Koumoto, J. Appl. Phys. **100**, 096105 (2006).
[23] G. Kresse, J. Hafner, Phys. Rev. B **47**, 558 (1993); **49**, 14251 (1994).
[24] G. Kresse, J. Furthmüller, Comput. Mater. Sci. **6**, 15 (1996); Phys. Rev. B **54**, 11169 (1996).
[25] J. P. Perdew, J. A. Chevary, S. H. Vosko, K. A. Jackson, M. R. Pederson, D. J. Singh, C. Fiolhais, Phys. Rev. B **46**, 6671 (1992).
[26] P. E. Blochl, Phys. Rev. B **50**, 17953 (1994).
[27] J. K. Burdett, T. Hughbandks, G. J. Miller, J. W. Richardson, J. V. Smith, J. Am. Chem. Soc. **109**, 3639 (1987).